Bed load transport and incipient motion below a large gravel bed river bend

Francisco Núñez-González*, Albert Rovira** and Carles Ibàñez**

*Leichtweiss-Institute for Hydraulic Engineering, Technische Universität Braunschweig, Braunschweig, Germany

**Aquatic Ecosystems Unit, IRTA, Apartat de correus 200, 43540 Sant Carles de la Ràpita, Catalonia, Spain

Abstract

A new data set of bed load measurements in a cross-section at the exit of a river bend is presented. Data are analyzed to identify processes that contribute to the morphodynamic stability of gravel bed meanders. It is shown that boundary shear stress and bed material texture are strongly coupled, resulting in an almost equal mobility at incipient motion over the bend point bar in relation to channel flow stage. Conversely, for conditions above bankfull an excess of fine sediment towards the inner-bank, likely related to more intense crosswise flux and grain size sorting, results in size selective transport in relation to the local bed material. We suggest that bed armoring and structuring, as well as crosswise sediment flux, add stability to the outer-bank pool, while the point bar is eroded by large floods and restored by moderate flows. Results reveal the strong feedback of processes at different scales promoting stability at bends of gravel bed rivers.

1. INTRODUCTION

A requirement for the morphology of a meander to remain stable is that the sediment supplied upstream must be expelled at the same pace downstream at the exit. If different grain sizes follow different pathways as they move through the bend, some processes and channel adjustments must act to promote the movement of all grain sizes at the same rate as they are supplied upstream, for varying flow conditions (Clayton & Pitlick, 2007). Identification of these processes and adjustments, with their relative significance, is of special importance in the context of anthropogenic climate change and the likely changes

on the hydrological regimes (e.g., Kundzewicz et al., 2007) and sediment yield at the catchment scale (Goode et al., 2012). The question arises, then, whether a change in the frequency and magnitude of river run-off and sediment supply would lead to channel instability in gravel-bedded river meanders.

Recent advances in physical and numerical modeling of meandering rivers have given valuable insight on the conditions needed to sustain meander dynamics. These advances have contributed to understand the controlling mechanisms in meander migration rate, sinuosity, floodplain formation and planform morphodynamics (e.g., Braudrick et al., 2009; Parker et al., 2011; Van Dijk et al., 2012; Schuurman et al., 2015). Nevertheless, knowledge gaps remain, particularly for recognizing whether meander dynamics for sand beds can be extended to non-uniform sediment beds, or in this case, if the dynamics is affected by different sediment sorting and mobility conditions. For instance, in gravel bed rivers changes in sediment supply exert a control on the surface structure of the river bed (e.g., Nelson et al., 2009; Ferrer-Boix & Hassan, 2014). Therefore, it is not clear if the dynamics of gravel bed meanders is affected by sediment supply in the same way as it has been observed in sand-bed streams, where high sediment supply is related to larger meander cutoff and migration rates (Constantine et al., 2014).

In meander bends the flow is characterized by a cross-stream motion, often described as a three-dimensional helical flow (Engelund, 1974; Smith & McLean, 1984). This helical flow is related to the curvature of the channel and the width-to-depth ratio (Lanzoni et al., 2006; da Silva et al., 2006; Termini & Piraino, 2011). For high width-to-depth ratios convective accelerations have a predominant influence on the velocity field (Dietrich & Smith, 1983; Termini, 2015), while for small width-to-depth ratios it is the cross-circulation that mostly determines the characteristics of the downstream velocity pattern and shear stress distribution (Blanckaert & Graf, 2001; da Silva, 2015). Due to this, the pattern of flow in bends is strongly linked to flow stage, with the morphological adjustments associated to an equilibrium flow condition (Dietrich & Whitting, 1989). Although field studies have confirmed this dependence on flow stage for morphological changes over point bars (e.g., Kasvi et al., 2013; Lotsari et al., 2014), the combined role of flow stage, bend geometry and the history of flow conditions on bar formation still needs to be

clarified, especially in gravel bed rivers where coarse and fine material contribute to bar construction.

As fine and coarse materials move through a bend they are segregated, resulting in the consistent pattern where coarse material is directed to the pool and fine material outwardly toward the point bar (Parker & Andrews, 1985; Bridge, 1992; Julien & Anthony, 2002). This process overlaps with other sorting processes that are also common in straight reaches, such as armouring and hiding-exposure. A response of a straight channel to achieve stability can be through selective lateral bed load transport and changes in surface texture, as reported by Nelson et al. (2010) in flume experiments with alternate bars. Varied shear stress driving sediment sorting in straight reaches, however, may not be as strong as in meanders (Lisle et al., 2000), where channel curvature and bed topography force strong spatial divergences in shear stresses, fractional sediment transport rates and bed material size (Dietrich & Smith, 1984; Clayton & Pitlick, 2007). A common sequence in the mobility of sediment mixtures reported for straight reaches considers that sediment transport evolves with flow stage from partial mobility, when only a portion of the grains on the bed surface are in motion (Wilcock & McArdell, 1993); to size-selective transport, when coarser sizes are in a lower proportion in the transport rates than in the bed (Parker, 2007); and finally to equal mobility, when the proportion of each size in the transport is equal to its availability in the bed material (Parker et al., 1982). Clayton & Pitlick (2007) recognized that analogous stages of sediment mobility occur spatially across the bed of a gravel bed river bend, from partial transport of coarser particles at the inner region of the bend, to full mobility at the outer region. Clayton & Pitlick (2007) argued that this crosswise transition leads to dynamic stability at the bend reach scale over long timescales, through a roughly equivalent bed load volume being transported by the inner, middle and outer regions of the channel. Furthermore, they suggested that armouring of the outer region of bends (the pool) would increase with bend curvature, so that coarse grains are more available to transport during high flows. This same feature has been recognized in recent field measurements at a river confluence (Martín-Vide et al., 2015). Nevertheless, differences in grain size mobility at different flow stages across a large gravel-river bend have not been thoroughly described.

The aim of this study is to identify at both local and cross-section scale, the sediment transport processes that contribute to the morphological stability of a large river bend with poorly-sorted material. We assume that the same processes acting in straight reaches are also fundamental for the stability at the local, cross-sectional and reach scales of a river bend. Analyses are based on intensive field observations of bed load and bed material collected at three sampling verticals placed at the exit of the bend section. Of particular interest are the incipient motion, derived from the maximum collected size, and the selective transport, derived by comparing bed material and fractional transport rates. The new data set provides a particular opportunity to analyze the spanwise variation in boundary-shear stress, bed material texture, and sediment mobility for a large range of discharges in a large gravel-bed river bend. Previous studies on sediment transport dynamics in river bends have been mostly focused on sand bed channels with relatively small width-depth ratios (Dietrich, 1987). Bed material is composed of sand and gravel in the study reach here, with width-to-depth ratios larger than 30. Thereby, the new data give an insight on conditions not investigated previously.

2. STUDY AREA

The study has been carried out in the lowermost parts of the Ebro River during the hydrological period 2007-2015. The Ebro river basin (85,530 km^2) is located in the northeast Iberian Peninsula (Fig. 1). It covers the south-facing slopes of the Cantabrian Range and the Pyrenees (in the northern part of the basin), and the north-facing slopes of the Iberian Massif in its southern part. At present, 57% of the total annual runoff of the Ebro river basin is impounded by close to 200 dams. This is a much higher rate of impoundment than that typically encountered in more humid regions and for catchments of similar size (i.e., 5 to 18% in the river Rhine, Elbe and Wessem [Vericat & Batalla, 2005]). Virtually, all dams were built during the twentieth century, especially in the period 1950-1975 when 67% of the total storage capacity was constructed. The largest system of dams (formed by the Mequinensa-Riba-Roja-Flix dams, Fig. 1), is located 100 km from the river mouth. Downstream of the reservoirs water is used for hydropower production and the cooling of a nuclear plant, but the main water use is for agricultural purposes. Almost one-

119 half of the mean annual water yield of the river basin is extracted from the streams and does
120 not return to the water system (Tábara et al., 2008).
121

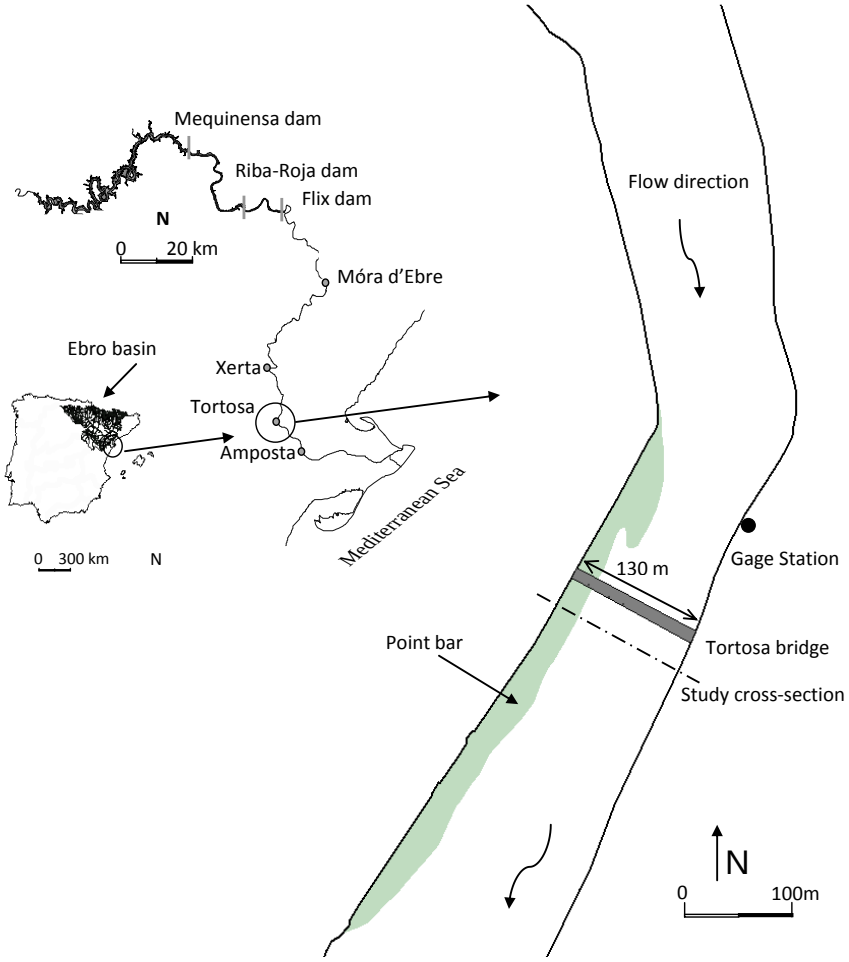

122 Figure 1. Location and characteristics of the study site.
123

124 The study section was located in Tortosa (drainage area 83,093 km^2), in a cross-
125 section placed 170 m downstream of the apex of a moderately sharp river bend (radius of
126 curvature/channel-width ≅4) (Fig. 1). The river there is channelized preventing both the
127 lateral mobility of the riverbanks and the overflow on the alluvial-plain. At the right-bank a
128 point bar is well-developed, mainly composed of unconsolidated coarse and medium gravel
129 with a median bulk particle size D_{50} computed at 16 mm. Bed material is extremely poorly
130 sorted. The mean hydraulic-channel slope is estimated at 0.0005. Bankfull discharge
131 (≅1,100 m^3/s, based on 1.5 years return period) is equaled or exceeded 3.5% of the time
132 (period 1968-2004) (Batalla et al., 2004). For the post-dam period, maximum peak

discharge recorded in Tortosa was 3,300 m^3/s (25 years return period), while during the study period the maximum peak discharge was 2,025 m^3/s (4 years return period) (see Fig. 2).

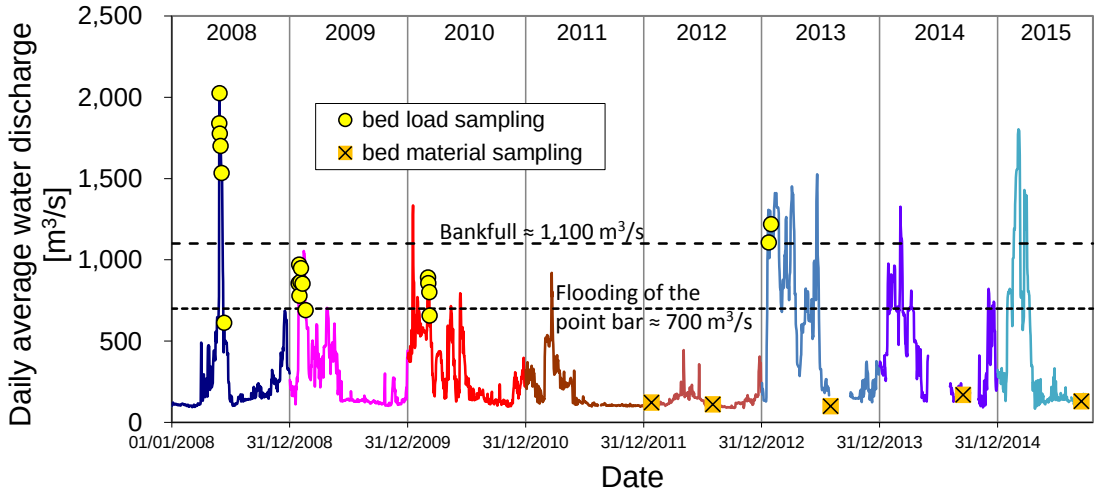

Figure 2. Average daily water discharge during the study period.

3. METHODS

3.1 Sampling verticals

Four sampling stations (or verticals) were set in the studied cross-section. Verticals were placed at 25, 59, 74 and 108 m from the left-bank (outer or concave bank), respectively designated as: Outer-bank (Ob), Central-channel (Cc), Inner-bank - Central-channel (Ib-Cc), and Inner-bank (Ib) (Fig. 3). These locations correspond to 19%, 45%, 57% and 83% of the 130 m channel width defined by the left and right vertical walls, which encroach the reach for flows larger than roughly 700 m^3/s. The sampling verticals were meant for an even distribution over the cross-section, while avoiding the potential effects of the bridge piers located 25 m upstream. The influence of the 5 m-wide piers was negligible, since the sampling verticals were more than 14 m away from them, and the downstream distance was far enough from their wake (the wake of rectangular piers with rounded nose, as in the study site, is limited to a distance of one pier width in shallow flow, e.g., Lima, 2014).

Besides, there was no evidence of abrupt changes in the bed elevation at any of the verticals, which could be related to local scour effects from the piers.

The cross-section was surveyed in June 2008 and August 2013. In the first field campaign, four extra cross-sections distributed along the bend were also surveyed (Fig. 3). Data were obtained by means of a digital eco-sounder model BioSonics DT-X (in the wet area), and a topographic total station (in the dry area). In order to link both data sets, a minimum of 3 coincident (overlapped) points were measured with both devices.

3.2 River bed material and bed load

River bed material was annually sampled from 2012 to 2015, mostly during summer season before the rainy period (see Fig. 2). Bed samples were taken by scuba divers since water depths in the sampling verticals ranged from almost 1 m in the Ib-Cc to up to 5 m in the Ob vertical. No standard methods are available for underwater sampling in gravel bed rivers. Thus, for the bed-surface material pebble counts were applied as it is normally recommended in wadable streams (e.g., Bunte & Abt, 2001). At each vertical, a minimum of 200 pebbles were collected from the bed surface. The sampling interval was large enough to avoid serial correlation (Church et al., 1987). For the bed-subsurface material bulk samples were collected within the area covered by the pebble counts. Accordingly, bed surface particles were removed to a depth of about the D_{90} of surface grains, and then the material below the surface was sampled to a depth of about two particle diameters. Subsurface material was taken using a scoop sampler, following Billi & Paris (1992), who reported the collection of river bed particles in deep water by divers with that method. Sample weight ranged between 15 and 48 kg, with the coarsest particles making up no more than 1% of the total weight of the sample (Church et al., 1987). Particles below 32 mm were dry-sieved in the laboratory and analyzed for 1ϕ intervals, while material greater than 32 mm was measured in the field by means of a template.

Bed load was sampled during 4 floods recorded from 2008 to 2013. Samples were taken during 19 days: 6 in 2008; 7 in 2009; 4 in 2010; and 2 in 2013 (see Fig. 2). The highest flood sampled was that of 2008 when sampling included the peak discharge of 2,025 m^3/s. Direct observations in the field revealed that the incipient motion of riverbed particles occurred at a discharge of around 620 m^3/s.

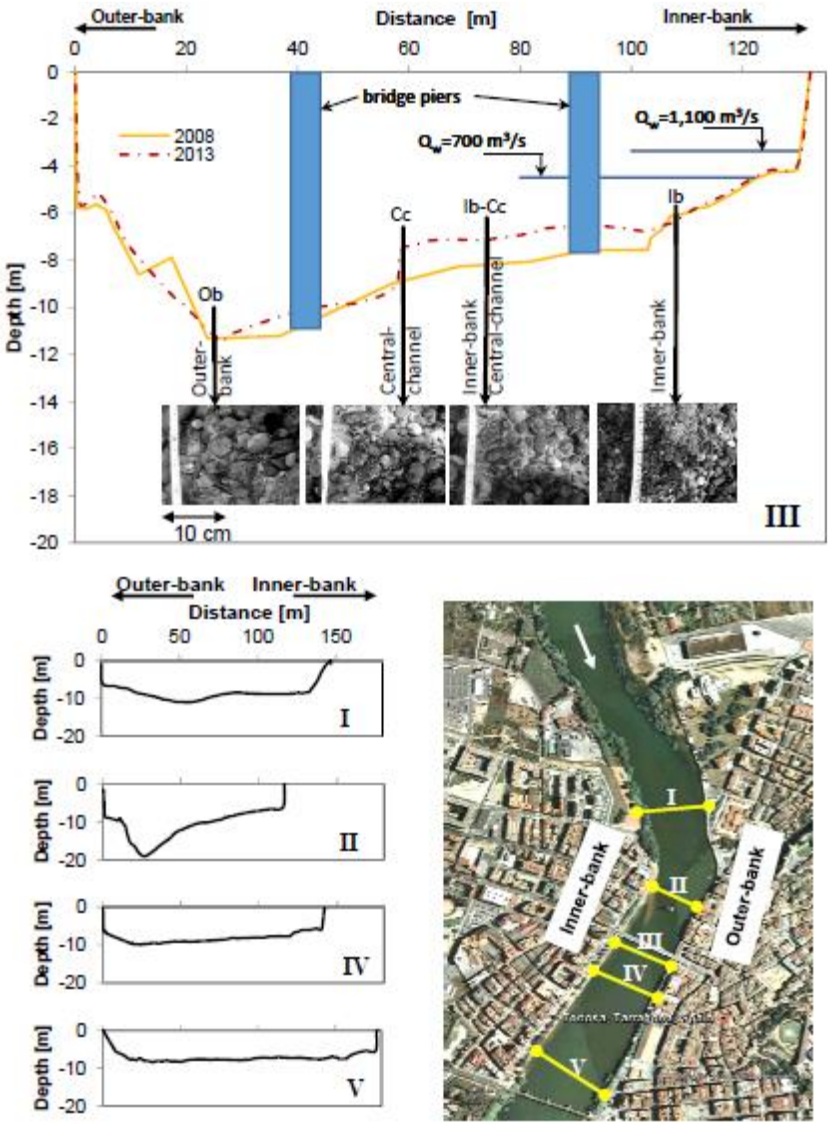

Figure 3 Cross-section of the study site for years 2008 and 2013 (above), and cross-sections along the bend for year 2008 (below). Q_w refers to water discharge. Photo taken from GoogleEarth.

Bed load samples were taken at the Ib, Ib-Cc and Cc verticals. Unfortunately, sampling at the Ob was not possible because of the extreme flow conditions (e.g., mean flow velocities recorded for a discharge of 770 m^3/s were as high as 2.5 m/s), and because the massive floating litter (e.g. woody debris and macrophytes) prevented us to carry out the sampling under safety conditions. In addition, the Ib vertical was only sampled in 2008 since it was active (in terms of bed load transport) at discharges above 1,700 m^3/s.

195 Samples were collected by means of a Helley-Smith sampler (29 kg weight, 76.2
196 mm inlet, expansion ratio [exit area/entrance area] 3.22, and mesh size diameter 0.45 mm).
197 Although some bias has been recognized for Helley-Smith samplers toward
198 overrepresentation of sand and fine gravel (e.g. Sterling & Church, 2002; Bunte et al.
199 2008), it is still a good option for sampling sand and gravel loads according to the high
200 sampling efficiencies found by several authors (e.g., Hubbell, 1987; Emmett, 1979), and
201 due to the lack of other reliable samplers to be used in relatively deep waters. Nonetheless,
202 for our study site, it must be expected that the load of the coarsest sizes of the river bed
203 could be undersampled (D_{90}= 53 mm for the coarsest grain size distribution of bed
204 material), and that the size of the inlet would set a cutoff size, so that the least frequent
205 coarse particles in the bed would be eliminated from the load (size of the coarsest particle
206 found on the bed surface was 85 mm, i.e., larger than the sampler inlet).
207 For discharges lower than 1,500 m^3/s bed load sampling was performed from a boat.
208 At each sampling vertical the boat was moored to an anchor with a buoy tied at the end of a
209 rope. The anchor was kept fixed at the same location for the whole sampling day. This
210 procedure ensured that samples were always taken approximately at the same verticals of
211 the cross-section. Once the boat was moored, the bed load sampler was carefully lowered
212 by means of a small crane. When the sampler was placed over the riverbed, the crane cable
213 was kept loose enough to avoid lifting of the sampler from the bed surface.
214 For flows larger than 1,500 m^3/s, the bed load sampler was lowered from the bridge
215 using a mobile crane placed at 8 m above the water level. Especial care was taken to locate
216 the sampler at the same positions as for measurements carried out from the boat. Either for
217 sampling from the boat or from the bridge, there were no means to check that the sampler
218 was lying on the stream bottom without any gap effect, or that shoveling was avoided.
219 Since the direct deployment of the sampler on the channel bed represents one of the largest
220 sources of bias of Helley-Smith samplers (Vericat et al. 2006; Bunte & Abt, 2009), the
221 collected data may contain some added scatter due to these drawbacks. Accurate estimates
222 of the bed load size distribution in gravel bed rivers require very long sampling times
223 (Dietrich & Whiting, 1989). Thus, in order to obtain representative samples, bed load
224 measurements during each sampling day were repeated from 6 to 10 times in a given
225 vertical. Not all the samples were obtained consecutively in the same vertical, but in

sequences of two consecutive measurements on each vertical, and in series of sequences over the verticals of the entire cross-section (traverses). Three series were measured for the highest discharges (> 2,000 m^3/s), and four series for discharges lower than 2,000 m^3/s, except for one sampling day for which five traverses were carried out. Sampling was always performed from the right- to the left-bank. Once the first traverse was finished, the second series started from the first vertical again. Approximate duration times of the different stages of a traverse are shown in Table 1. Each sampling day and before starting the first traverse, a suitable sampling duration was estimated to ensure that no more than 50% of the sampler bag would be filled. With that purpose, the bed load sampler was placed over the streambed during 2 minutes, and then consecutive time increments of one minute were carried out to know when the bag would be filled up to 50%. Thereby, sampling durations ranged from 2 to 5 minutes. A total number of 288 individual bed load samples, 14 from Ib, 144 from Ib-Cc and 130 from Cc, were dried, weighted and sieved at 1 ϕ intervals for grain size analysis at the laboratory, as described by Bunte & Abt (2001). Unit total bed load rates were obtained from $q_s = w_s / [t_s b_s \eta]$, where b_s is the width of the sampler, t_s is the sampling duration, w_s is the dried weight of the sample, and η is the efficiency of the sampler, considered as $\eta=1$. Similarly, fractional transport rates were obtained from $q_{si} = w_{si} / [t_s b_s \eta]$, where the subscript i denotes a specific grain size class.

Table 1. Main features of the bed load sampling

Sampling features	Duration
Total sampling duration (1)	2-3 hours
Sampling interval between verticals (2)	15-30 minutes
Sampling interval between samples (3)	4-8 minutes
Sampling time (4)	2-5 minutes
Number of series (traverses)	3-5 times

(1) Total sampling duration per day

(2) Interval that elapses between consecutives samples from one vertical to another vertical

(3) Interval that elapses between consecutive two samples taken at the same vertical

(4) Total time that the sampler remains over the bed

3.3 Estimation of hydraulic parameters

Water discharge was obtained from the gauging station located 130 m upstream from the cross-section. The station uses a stage-discharge rating curve. In general terms, no significant water discharge variations were observed within each sampling day (variations were 4 m^3/s on average, with a maximum value of 11 m^3/s), due to the flow regulation from the upstream reservoirs. For discharges lower than 1,250 m^3/s, water depth and flow velocity were measured at least three times at the same verticals of bed load sampling (measurements were not possible for higher discharges for safety reasons). Flow velocity was measured at 60% of the water column depth by means of a current-meter (model Valeport Braystoke BFM001). Water depth and flow velocity measurements were also carried out during the same period for some discharges below incipient motion (i.e., $<\cong$620 m^3/s).

Bed shear stress has been computed assuming a logarithmic distribution of flow velocity and no influence of channel walls, so that $R_h = h$:

$$\tau_o = \rho \left(\frac{V}{\frac{1}{\kappa} ln \frac{11h}{k_S}} \right)^2 \qquad (1)$$

where h is the water depth; k_s is the equivalent roughness, considered as $k_s = 2D_{90Sur}$, being D_{90Sur} the grain size for which 90% of the particles on the surface layer are finer; V is the measured mean flow velocity; κ is the von Karman constant considered as 0.4; and ρ is the water density. Bed shear stress computations were also performed with the *single-velocity method* suggested by Dietrich & Whiting (1989), using near-bed velocity measurements (30 to 40 cm from the bed level) available for a number of limited days. Stresses computed with this method were systematically higher, in average from 8 to 20%, and the trends with respect to water discharge exhibited a larger scatter. Therefore, this data were not used further. Results obtained from Eq. (1) were used to compute the Shields stress for each sampling vertical as follows:

$$\tau_* = \frac{\tau_o}{\rho g (S_s - 1) D_{50}} \qquad (2)$$

where D_{50} is the median diameter of the bed material; g is the acceleration of gravity; and S_s is the relative density of the sediment taken as equal to 2.65.

3.4 Largest-grain method

The incipient motion of grain size fractions was calculated at each vertical (except for Ib where the short number of samples made this method unfeasible) by means of the largest-grain method (or competence method) (Andrews, 1983), using the maximum grain size trapped in all samples collected during a single day. This method associates the critical shear stress and the largest grain D_{max} in the mixture collected (Andrews, 1983; Carling, 1983), by assuming that the flow of the day was at the threshold of motion for that grain size. In this analysis, the dimensionless critical shear stress (τ_{*ci}) is usually plotted against the relative particle size (D_{max}/D_{50}) to obtain the expression (so-called *hiding function)*:

$$\tau_{*ci} = \tau_{*c50}\left(\frac{D_i}{D_{50}}\right)^{-b} \qquad (3)$$

where D is grain size, τ_{*c} is the critical Shields stress for inception of motion, and subscripts i and 50 denote a given grain size fraction and the median particle diameter, respectively. The exponent b ranges from 0, in case of size-selective entrainment as defined by Shield's relation, to 1 for equal mobility of all grains found on the bed (Andrews & Parker, 1987). Common values of b obtained from measurements by different authors range from 0.65 to 1.0 (Parker et al. 1982; Andrews, 1983; Komar, 1987; Ashworth & Ferguson, 1989).

We chose the largest-grain method instead of the reference transport method (Parker et al., 1982; Wilcock & Southard, 1988) because of the limited range of low discharges sampled (that could introduce some bias in the results when applying the reference transport method), and because we are confident enough about the representativeness of the D_{max} from the samples, since it was obtained from a relevant number of collected samples (in average, 8 samples per day and vertical). As previously indicated, water discharge remained relatively steady during each sampling day. This allowed the association of all samples collected during one day to a single discharge.

Several studies (e.g., Wilcock, 1992; Batalla & Martín-Vide 2001; Church & Hassan, 2002) have pointed out two weak points, at least, of the largest-grain method: i) results are based on the largest trapped particle, which does not necessarily reflect the maximum mobilized particle in the bed because coarse size fractions might be poorly sampled; and ii)

the intercept parameter of the hiding function is very sensitive to the characteristic size used in the coefficient of Eq. (3). To minimize the effects of i), long sampling durations are required to increase the chance for coarse size fractions to be trapped by the sampler (Whitaker & Potts, 2007). By considering a unique grain size per day, we indeed increased the sampling duration to enhance the chance of trapping the coarsest grains in motion. In addition, there is some added bias related to i) due to limitations of the sampler opening. Notwithstanding, this represents a very small fraction of the bed material in our case, since for the bed material grain size distributions (GSD) of all the verticals $D_{95} > 64$ mm, while the Helley-Smith opening was 76.2 mm. In relation to ii), the analysis was first performed using the surface median diameters in Eq. (3), but it was then repeated using the subsurface diameters; the effect was negligible regarding exponent b, while for τ_{*c50} some differences were found, as described in Section 4.5.1.

4. RESULTS

4.1 Bed level adjustments

Figure 3 shows that between 2008 and 2013 the point bar located at the study cross-section aggraded ca. 0.8 m in average. Bed level rose up to 1.2 m at the lateral edge of the bar (where the Cc vertical is located), while at the middle parts (in the Ib-Cc vertical) the increment was ca. 0.8 m. Water depth measurements revealed that these bed level changes took place during the 2009 and 2013 floods. In the Ib-Cc the bed level aggraded between 0.4-0.5 m in 2009, and between 0.3-0.4 m during the large event recorded in 2013. This pattern was also observed in the Cc vertical where the river bed aggraded 0.5 m in the 2009 flood, and 0.7 m in the 2013 event. In contrast, during the large 2008 flood the point bar was scoured between 0.7-1.0 m. This result is based on the diachronic analysis of the relationship between water depth and water discharge (analysis not shown here), plus field evidences from visual inspections. From this analysis it was found that, for the same water discharge and sampling vertical, recorded water depths were lower before the 2008 flood than after this large event. Consequently, it might be inferred that in the study section a general cycle of erosion-aggradation of the point bar exists, with a similar return period as the large flood of 2008 (4 years).

4.2 Bed material

Particle sizes found in bed material samples ranged from 0.045 to 85 mm. The bed surface was, in general terms, gravel dominated, with the presence of small irregular sand patches. Altogether, no imbrication or structuring of the superficial particles over the point bar was noticeable. This could probably be related to the aggradation of the bar between 2008 and 2013, leading to the recent formation of the deposit and the short exposure of the particles to a varied range of competent discharges.

Table 2. Main parameters of the superficial and subsuperficial grain size distributions of the river bed particles in the studied cross-section. D_g and σ_g are the geometric mean size and standard deviation, respectively; D_x is the grain size diameter for which x% of the particles are lower by weight.

Sample	**Vertical**	**Sand content (% < 2 mm)**	**D_g [mm]**	**σ_g [mm]**	**D_{16} [mm]**	**D_{50} [mm]**	**D_{84} [mm]**	**D_{90} [mm]**
Surface	Ib	-	12.6	1.7	6.9	12.3	23.7	27.5
	Ib-Cc	-	14.0	1.8	8.2	14.3	26.2	29.2
	Cc	-	25.2	1.6	16.6	24.8	44.0	51.2
	Ob	-	23.9	1.6	15.4	23.9	42.2	50.1
Subsurface	Ib	27.5%	5.1	5.2	0.5	9.1	23.9	28.9
	Ib-Cc	10.5%	9.0	3.1	3.3	11.5	24.9	28.6
	Cc	1.8%	21.1	2.2	11.2	22.8	44.2	52.8
	Ob	0.0%	19.7	1.6	11.0	20.2	31.1	39.4
Surface/Sub-surface (truncated at 4 mm)	Ib	-	0.88	0.92	0.97	0.88	0.84	0.86
	Ib-Cc	-	1.05	0.95	1.15	1.03	0.99	0.99
	Cc	-	1.11	0.87	1.39	1.07	0.99	0.96
	Ob	-	1.21	0.99	1.40	1.18	1.36	1.27

The analysis of the GSDs of the surface and subsurface material revealed no significant differences between the four sampled years. The median diameters were quite

stable, and no clear trends over time were evident. Hence, samples obtained at each vertical for all the sampled years (from 2012 to 2015) were combined into two unique averaged GSDs (one for the surface layer and another for the subsurface particles), and hereafter used for analysis. The main parameters of the obtained GSDs are shown in Table 2.

The comparison between bed surface and subsurface material is presented in the last four columns of Table 2. For their comparison, the minimum size class of bed material was truncated at 4 mm in order to avoid bias due to the limitations of the pebble-count method used for sampling the superficial bed material. Results show that at the Ib vertical the bed surface was finer than the subsurface (yielding an armoring degree lower than 1). In contrast, at the Ob this relation is reversed; the bed surface was coarser than the subsurface layer exhibiting, albeit subtle, a certain degree of armoring (estimated at 1.3). Finally, the Ib-Cc and Cc verticals appear as transitional points in which both distributions (surface and subsurface) only match for the coarser grain sizes.

4.3 Hydraulic variables

In spite of the aggradation of the point bar observed between 2008 and 2013, no significant changes in the relation between flow velocity and water discharge were observed over time. As expected, maximum values of water depth, flow velocity and bed shear stress occurred at the Ob vertical with a progressive decrease toward the inner bank, where minimum values were recorded.

Figure 4 shows the variation of the bed shear stress τ_o and Shields stress τ_* with increasing water discharge. Shields stress was computed based on the median diameter of the surface material $D_{50,Surf}$. Results show that for the same water stage, Shields stress values in the Ob vertical (that is, at the outer part of the river bend) are, in average, 19% larger than in the Ib-Cc and Cc verticals. Conversely, τ_* in the Ib vertical is one order of magnitude lower than in the other analyzed points. In addition, we observe that Shields stress values in the Cc and Ib-Cc verticals collapse into a single trend. The similarity between both sampling verticals (the Ib-Cc and Cc) is explained by the coinciding ratios $\tau_o/D_{50,Surf}$. Hence, it is fulfilled that:

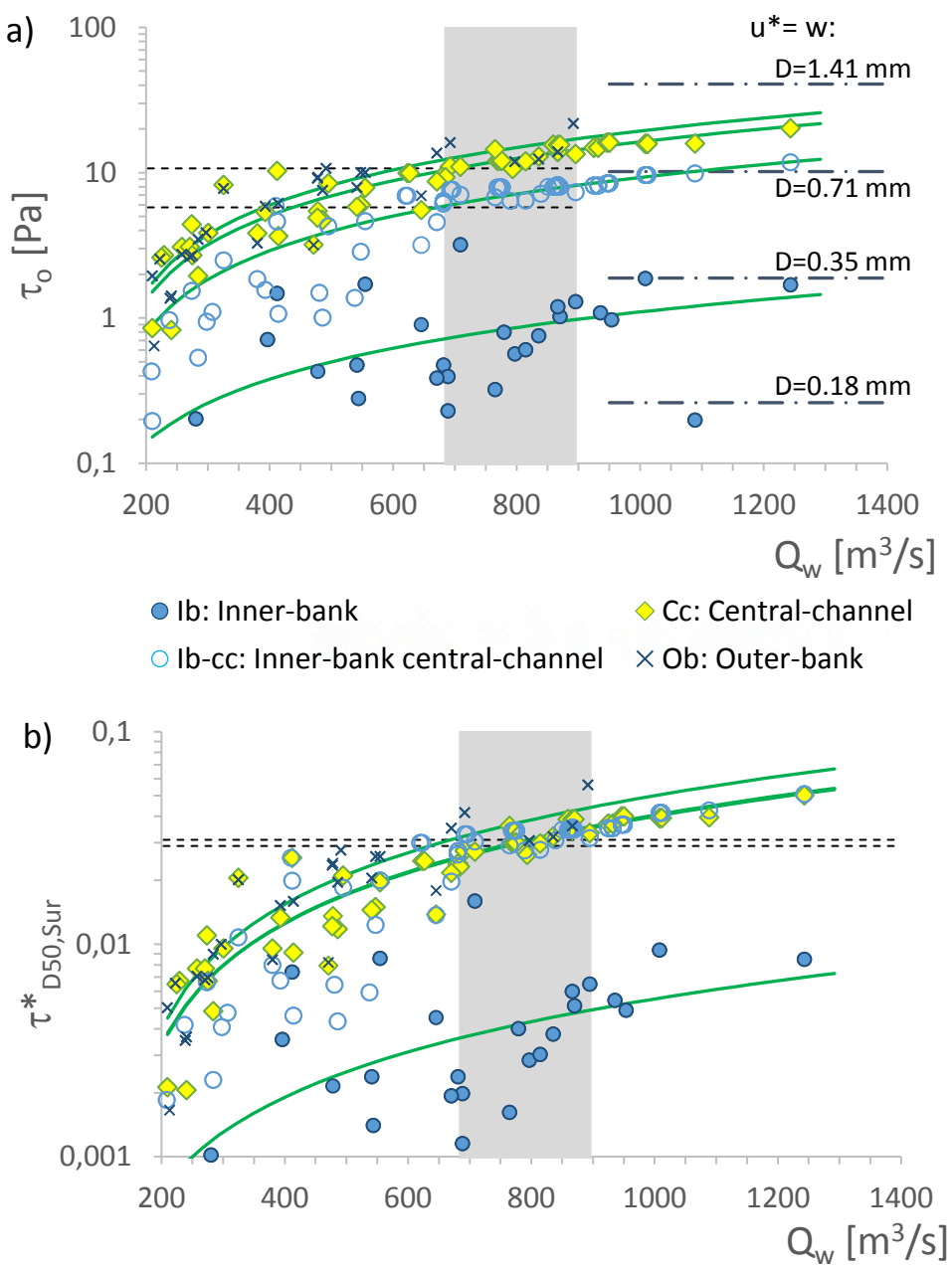

Figure 4 Variation of (a) bed shear and (b) Shields stress with water discharge. Continuous lines are the best-fit lines to the data of each measuring vertical (parameters shown in Table 3). Dashed lines indicate the critical stress of the median diameters in the Ib-Cc and Cc verticals; and dashed-dot lines in (a) indicate the conditions for suspension of grain size D when shear velocity u* equals the settling velocity w of grains, according to the criterion of Dietrich (1982).

$$\frac{(\tau_0)_{Cc}}{(\tau_0)_{Ib-Cc}} = \frac{(D_{50,Surf})_{Cc}}{(D_{50,Surf})_{Ib-Cc}} \approx 1.75 \qquad (4)$$

where the subscripts Cc and Ib-Cc indicate the Central-channel and Inner-bank Central-channel verticals, respectively.

Table 3. Parameters for the best-fit lines $\tau_o = b' + mQ_w$, shown in Figure 4a, and obtained by regressing local boundary shear stress against water discharge.

	Ib	**Ib-Cc**	**Cc**	**Ob**
b'	-0.10	-1.34	-2.42	-2.95
m	0.0012	0.0106	0.0187	0.0223
r	0.67	0.86	0.92	0.91

4.4 Bed load transport rates

4.4.1 Total bed load

Figure 5 shows the relationship between water discharge and unit bed load transport rates for samples collected during the period 2008–2013. The obtained plot shows the typical degree of scatter due to the pulsing and unsteady nature of the bed load processes in gravel bed rivers; yet some general trends can be traced. Bed load transport rates at the Ib vertical are two orders of magnitude lower than at the Ib-Cc and Cc verticals, while transport rates at these two latter locations are roughly of the same order of magnitude following similar trends. Figure 5 also reveals the existence of a small group of discordant data, located at the lower range of sampled discharges (see shadowed data points on the left part of Fig. 5). These values are exceptionally high for the magnitude of the corresponding discharges, lying outside the main cluster of data.

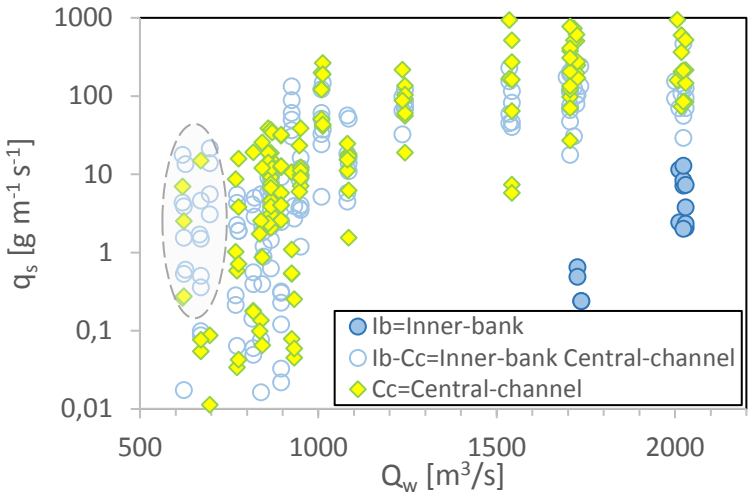

426

427 Figure 5 Relationship between water discharge and total bed load transport rate. Samples
428 were collected from years 2008 to 2013. Data points within the shaded region indicate
429 outlying behaviour.

430

431 Bed load rates have been plotted against bed shear stress in Figure 6. In the upper
432 panels of this figure, points identified as outliers in Figure 5 have been linked to the
433 sampling day when bed load samples were collected. It should be recalled that for safety
434 reasons, the hydraulic variables were only measured for flow discharges lower than 1,250
435 m^3/s. Hence, the number of data points drawn in Figure 6 is lower than in Figure 5. The
436 obtained plots show that the anomalous bed load transport data were collected in the
437 sampling days 6 (year 2008), 13 (year 2009) and 17 (year 2010), for the Ib-Cc vertical, and
438 in the sampling days 6 and 17, for the Cc vertical. For the Ib-Cc vertical, samples collected
439 during day 6 (year 2008) and day 13 (year 2009) clearly fit within the main data cluster.
440 Revision of the raw data revealed that flow velocities related to these latter samples, and
441 thus bed shear stresses, were unusually larger than the average trend for the Ib-Cc. In
442 consequence, for these points a change in the relation between channel-discharge and local
443 flow conditions, possibly triggered by morphological changes, might explain their
444 separation from the main cluster in the graphic. For data corresponding to day 17 in Ib-Cc
445 and for the outliers in Cc, a likely reason for their departure from the main trend may be
446 hysteretic phenomena related to the falling limb of the hydrograph.

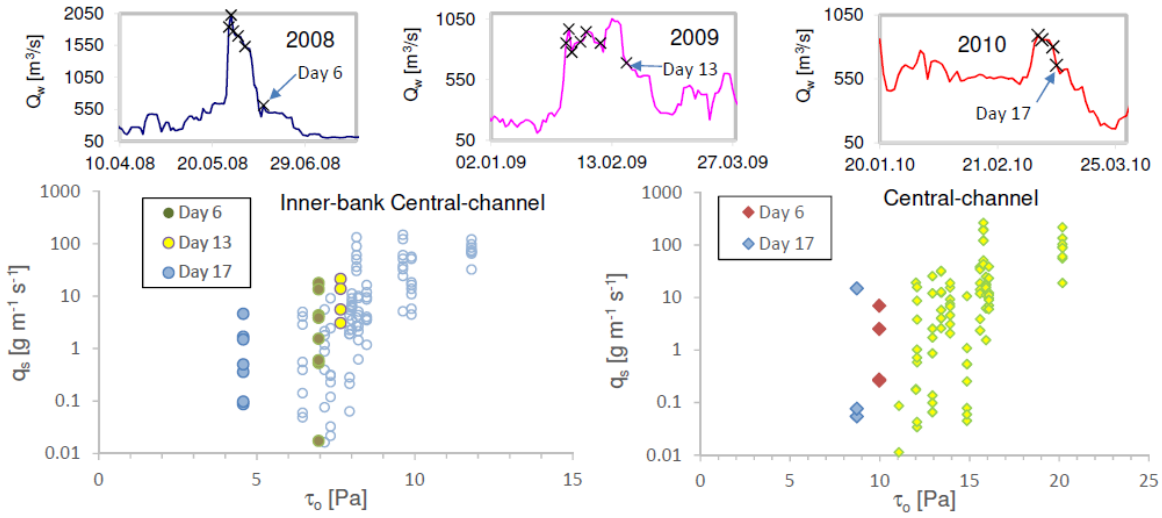

Figure 6 Bed load transport rates as function of bed shear stress. Data points with anomalous behavior are shown by colors in the plot. Upper panels show the location of these data points in the flood hydrograph. Crosses indicate days when bed load was measured.

4.4.2 Fractional transport rates

The largest particle captured in the sampler had a diameter of 75.7 mm, while the minimum size range considered for sieve analysis was from 0.25 to 0.5 mm. For the fractional transport rates analysis, the individual bed load samples were combined into seven classes of water discharge. Grouping served to eliminate the natural variability inherent to the transport processes in gravel beds (Reid & Frostick, 1986; Kuhnle, 1992; Powell et al., 1999), and enabled a straightforward identification of the average changes in bed load texture for the whole range of analyzed discharges. Water discharge was chosen over bed shear stress as a hydraulic variable in order to allow a direct comparison between sampling verticals, but also because bed shear stress was only available for discharges lower than 1,250 m^3/s. Samples pertaining to the days indicated in the upper panels of Figure 6, i.e., sampling days linked to the eccentric points in Figure 5, were analyzed apart, i.e., each as a class in itself.

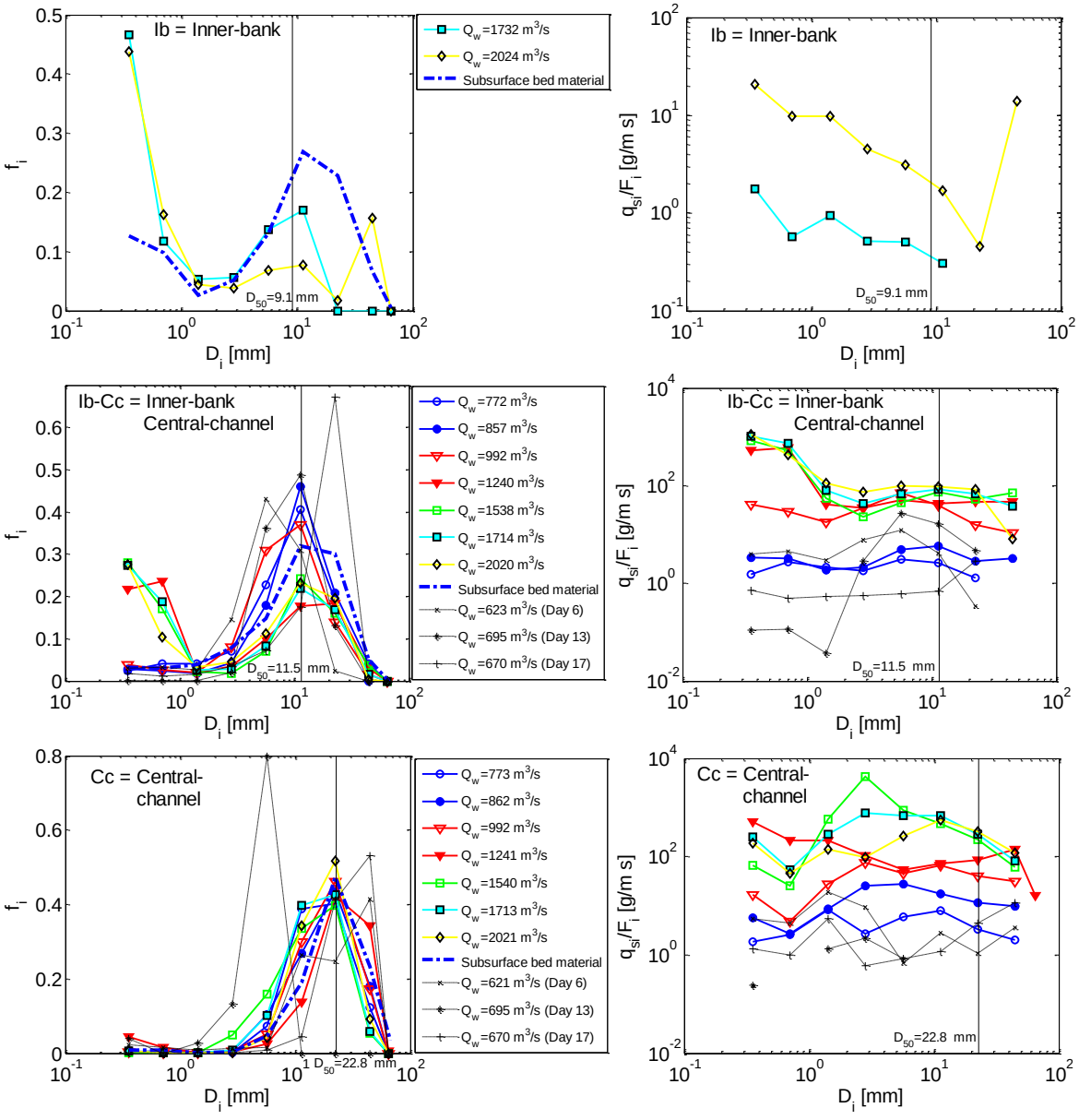

Figure 7 Frequency distribution of transported material grain sizes (left), and fractional transport rates for each grain size related to the relative abundance of each size fraction in the subsurface (right). Median diameters correspond to the subsurface material and water discharges correspond to the center of class discharge.

The GSDs for the combined bed load samples are shown in the left-hand side panels of Figure 7, where f_i is the fractional content of size i in each sample, calculated as $f_i=q_{si}/q_s$. For comparison, distributions of local average subsurface material are also drawn, as well

as the distributions for combined samples of each of the three days with anomalous data (see Fig. 6; days 6, 13 and 17). Overall, in the Ib-Cc and Cc verticals and for the whole range of sampled discharges, the mode of the subsurface material was conserved on the corresponding bed load distributions, with the exception of the low discharges corresponding to days 6, 13 and 17. In detail, we observe that at the Ib-Cc vertical almost all grain size fractions of the riverbed were mobilized for all of the competent discharges; except the grain sizes larger than 32 mm (equivalent to D_{95} of the bed material). Furthermore, for water discharges roughly exceeding 1,000 m^3/s, the distributions become strongly bimodal, with one mode in the sand fraction and one mode in the gravel range. This abrupt fining trend is striking, given that the most abundant size fractions in the fine mode correspond to those that are supposed to be transported in suspension for flow stages roughly larger than 1,000 m^3/s, i.e., D_i=0.35 mm and D_i=0.71 mm, as shown in Figure 4a. An effect of suspended material being captured when lifting the sampler is discounted, since the fine material was always evenly distributed in the mesh of the sampler. A superabundance of the same fine size fractions as in Ib-Cc was recorded in the Ib vertical as well, which is only active (in terms of bed load) for discharges larger than roughly 1,700 m^3/s. In this location the amount of fines in the two sampled flows exceeds by almost a factor of three the fines content in the subsurface material. In the Cc vertical fine material only represents a very small fraction of the bed load, and as such, the GSDs of the sediment in transport replicate to a great extend the GSD of the bed material.

Panels on the right-hand side of Figure 7 show the relative mobility of each grain size fraction in relation to its relative abundance in the bed material, for the same water discharge classes as in the panels on the left-hand side. The relative mobility is defined by the ratio q_{si}/F_i, where F_i is the relative frequency of the corresponding grain size fraction in the bed material. Subsurface samples were used for graphics in Figure 7. Nevertheless, no important changes resulted in the interpretation of the results whether using the surface or the subsurface sediment since superficial populations are, in part, reflected in the subsuperficial strata as previously indicated. Yet the use of the bulk material was preferred over the surface material due to the lack of the whole spectrum of grain sizes on bed surface samples, as a consequence of the intrinsic limitations of the pebble-count sampling method. For interpretation of the relative mobility curve for a given discharge class, an

508 almost constant value of q_{si}/F_i for all grain size fractions would mean equal mobility, i.e.,
509 that bed load has the same size distribution as bed material. Deviations upwards or
510 downwards would describe an overrepresentation or underrepresentation, respectively, of
511 the given size fraction in transport (that is selective-transport); and $q_{si}/F_i=0$ for any of the
512 grain sizes would mean partial-mobility, i.e., that not all the grain sizes in the bed material
513 take part in the transport.

514 In general terms, the right hand-side panels of Figure 7 show a widespread trend for
515 equal mobility in Ib-Cc and Cc, with the exclusion of data collected in days 6, 13 and 17.
516 Remarkable is the pattern already noticed in the panels to the left, for a sudden excess of
517 fines in Ib-Cc for discharges larger than 992 m^3/s, so that an outstanding selective transport
518 of the fine size fractions is evidenced. For Cc there is a slight overrepresentation of grain
519 sizes between 2 and 16 mm, particularly for flows larger than 1,241 m^3/s. On the other side,
520 in Ib selective transport of the fine fractions occurs for the two ranges of discharges
521 sampled, with an outlier for the coarsest size fraction.

522 Samples for days 6, 13 and 17 in Figure 7 show different trends with respect to the
523 rest of the data in Ib-Cc and Cc. Particularly, stands out that data pertaining to these three
524 days show some size-selective transport biased toward the coarser grains, even when the
525 related flow discharges and bed shear stresses were some of the lowest measured during
526 bed load sampling (Figs. 5 and 6).

527 **4.5 Incipient motion**

528 **4.5.1 Hiding functions**

529 The parameters for the hiding function given in Eq. (3) were obtained by regression
530 analysis based on data of maximum particle sizes in motion. This regression relationship is
531 highly sensible to the presence of outliers (Whitaker & Potts, 2007). To reduce this effect,
532 bed load data that showed an outlying behavior were excluded from the analysis (see
533 Section 4.4). These data correspond to samples collected during the falling stage of the
534 hydrographs (see Fig. 6) and, therefore, are not completely appropriate to analyze threshold
535 of motion conditions.

A requisite for the implementation of the largest-grain method is that particles coarser than grains in motion have to be available for transport in the river bed (Wilcock, 1988), i.e., the method must be applied only to flows not competent to mobilize the coarsest grain sizes in the bed. Therefore, for the incipient motion analysis we have only considered the sampling days in which the bed shear stress was lower than the lowest shear stress that would mobilize the maximum particle sizes caught by the sampler. The diameters of the largest particles trapped at the Ib-Cc and Cc verticals are 67 and 76 mm, which are entrained, respectively, at shear stresses of 8.5 and 15.6 Pa, corresponding to discharges of 950 and 864 m^3/s, respectively. Setting these values as an upper limit in the analysis, 9 maximum grain sizes were considered in the Ib-Cc and 8 for the Cc sampling vertical.

Shields stresses for the maximum grain sizes that meet the screening criterion described above are shown in Figure 8a, along with the best-fit hiding functions using the corresponding bed surface median diameter in Eq. (3). The resulting hiding functions for both verticals are almost identical. The exponent b is close to one, giving evidence of a trend toward equal mobility, i.e., bed shear stress for the threshold of motion is roughly independent of grain size. In addition, results reveal that Shields stress values for the median diameter in the verticals are highly similar (i.e., 0.029 and 0.031). Finally, the effect of using the subsurface instead of the surface median diameter in Eq. (3) is subtle, with a small increase of τ_{*c50}, being in this case 0.035 for Ib-Cc and 0.033 for Cc; but the exponent of the hiding functions remains the same.

Figure 8b illustrates the reduced hiding-exposure relations as a function of the grain size and the bed shear stress. For a direct comparison between both verticals, the Shields curve for uniform sediment suggested by Parker (2007), has also been plotted. In the Parker modified form of Shields' curve, τ_* equals 0.03 for the limit of hydraulically rough flows. In the obtained graph, the critical shear stress for the median diameters (interpolated and extrapolated from the hiding functions in the Cc and Ib-Cc verticals, respectively), plots over the corresponding values of the Shields' curve suggesting that at the local scale the median diameter controls the mobility of the entire sediment mixture. In addition, Figure 8b points out that for a given particle size, the critical shear stress in the Cc vertical is about twice the obtained for the Ib-Cc. Also, values of critical shear stress estimated for both

verticals are totally different to the value ascribed to the Shields curve, except for the local median diameter.

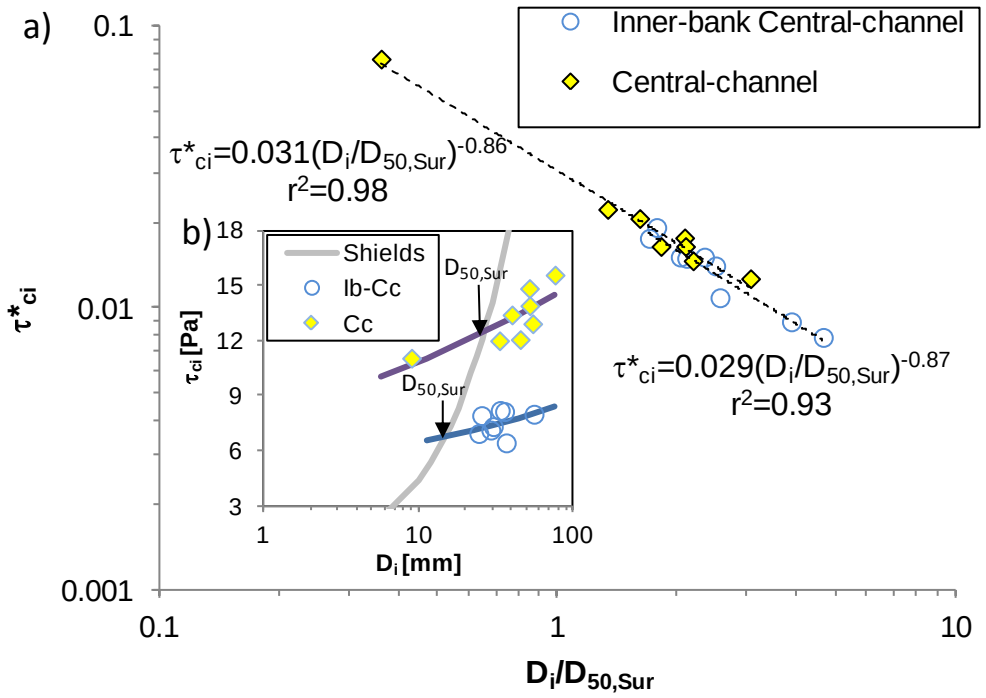

Figure 8 Incipient motion relationships obtained by the largest-grain method. (a) Hiding functions, i.e., the relation between critical Shields stress and the ratio i-th grain size fraction to median diameter; (b) critical bed shear stress to i-th grain size. Shields curve for uniform sediment is shown for comparison.

4.5.2 Critical water discharge

The results above showed that the hiding function in Eq. (3) is almost identical at the Cc and Ib-Cc verticals. Hence, if the critical Shields stress for the median diameter and the exponent b are considered to be approximately the same in both verticals, the ratio between the critical boundary shear stresses for a given grain size in the two verticals equals to:

$$\frac{\tau_{*ci(Cc)}}{\tau_{*ci(Ib-Cc)}} = \frac{\tau_{ci(Cc)}}{\tau_{ci(Ib-Cc)}} = \left(\frac{D_{50,Sur(Ib-Cc)}}{D_{50,Sur(Cc)}}\right)^{-b} = 1.75^{0.865} = 1.62 \quad (5)$$

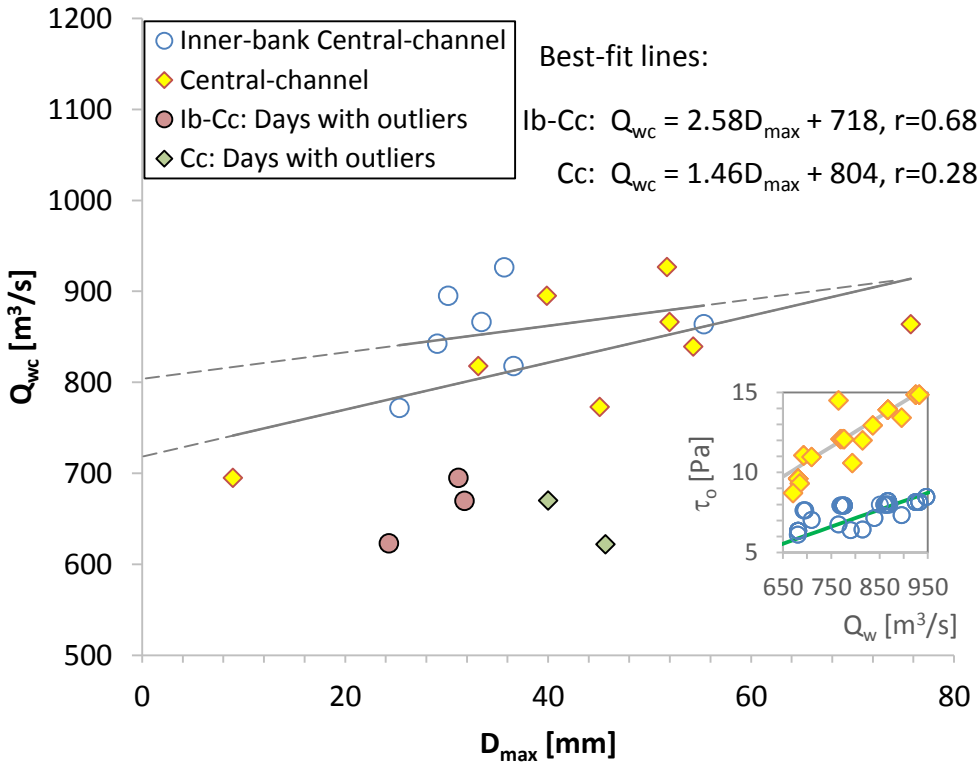

581

582 Figure 9 Water discharges for incipient motion Q_{wc} obtained from the largest-grain method.
583 The insert shows the variation of bed shear stress for the points in the main graphic at each
584 sampling vertical and for discharges < 1,000 m^3/s.

585

586 For a given water discharge, this value is in the same range as for the ratio between the bed
587 shear stress at the Cc and Ib-Cc verticals (Fig. 4), which has been found to be close to 1.75
588 (Eq.[3]). Therefore, the incipient motion for a given grain size would occur at very similar
589 discharges in the two analyzed verticals. This is well exemplified by plotting the grain sizes
590 obtained with the largest-grain method against the corresponding flow discharge for which
591 these diameters were sampled (Fig. 9). The resulting plot reveals the existence of a
592 relatively narrow region where incipient motion is most likely to occur. Indeed, data for the
593 two verticals (Ib-Cc and Cc) almost collapse displaying highly similar trends. Points
594 outside of this region correspond to the eccentric data related to waning flow conditions (as
595 illustrated in Section 4.4). Therefore, it can be stated that in both verticals incipient motion
596 for most of the grain size fractions in the bed is restricted to the same range of discharges,

which is approximately between 700 and 900 m^3/s. These values have been indicated in the shaded area of Figure 4 where dashed lines correspond to the critical shear stresses for the median diameters. These lines intercept the corresponding measured data points more or less in the middle of the shaded region, at nearly the same flow discharges for the two verticals, between 700 and 800 m^3/s.

The insert in Figure 9 shows the relation between the measured bed shear stress and the corresponding discharge in Ib-Cc and Cc for discharges lower than 1,000 m^3/s. The obtained plot points out a strong trend toward equal mobility in both verticals; even when for a given discharge the bed shear stress in Cc is almost twice that in Ib-Cc. Consequently, the movement of the same grain size in both locations would begin at nearly the same moment.

5. RELATIVE MOBILITY BETWEEN VERTICALS

The previous results give evidence of a sharp symmetry between the Cc and Ib-Cc sampling verticals for the incipient motion, resulting in a strong trend toward equal mobility. Next, we analyze if this symmetry is conserved at higher flow stages. For that purpose, the relative mobility between the measured verticals has been examined by means of a formal definition of relative mobility similar to that introduced by Parker & Klingeman (1982).

Consider two locations in the channel bed, A and B, that under the same water discharge are subjected to different boundary shear stresses, τ_{0A} and τ_{0B}, respectively. If a given grain size D_i is transported in A and in B at a volumetric bed load rate per unit width q_{siA} and q_{siB}, then the relative mobility $r_{i,AB}$ of material D_i in point A with respect to the same grain size material in the point B is:

$$r_{iAB} = \frac{q_{siA}}{q_{siB}} \qquad (6)$$

Hence, the mobility of the particles D_i in A is larger than the mobility of D_i in B only if $r_{i,AB} > 1$.

In order to formally implement the Eq. (6), a bed load function is required. We use the Meyer-Peter & Müller relation, which is often employed for bed load estimations in gravel bed rivers. This formula is commonly cast in the form:

$$q_{*i} = \alpha(\tau *_i - \tau *_{ci})^{\beta} \qquad (7)$$

where q_{*i} is the so-called Einstein number or intensity of transport for a given grain size i; α and β are constants; τ_{*i} is the boundary Shields stress; and τ_{*ci} is the critical Shields stress for grain size i. Yalin (1992) provided fundamental arguments to consider the exponent in Eq. (7) as equal to $\beta=3/2$. Finally, the intensity of transport is defined as:

$$q_{*i} = \frac{q_{si}}{F_i\sqrt{(S_S-1)gD_i^3}} \qquad (8)$$

where F_i is the fractional content of grain size i in the bed; g is the acceleration of gravity; q_{si} is the volumetric bed load rate per unit width; and S_s is the relative density of the sediment.

It can be shown, that using Eqs. (7) and (8), Eq. (6) can take the form:

$$r_{iAB} = \frac{F_{iA}}{F_{iB}}\left(\frac{K_o\tau*_{iB} - K_c\tau*_{ciB}}{\tau*_{iB} - \tau*_{ciB}}\right)^{\frac{3}{2}} \qquad (9)$$

where K_o and K_c are defined as:

$$K_o = \frac{\tau*_{iA}}{\tau*_{iB}} = \frac{\tau_{0A}}{\tau_{0B}} \qquad (10)$$

and

$$K_c = \frac{\tau*_{ciA}}{\tau*_{ciB}} = \frac{\tau_{ciA}}{\tau_{ciB}} \qquad (11)$$

where τ_{ci} is the boundary shear stress for incipient motion of grain size i.

Now, consider the verticals Ib-Cc and Cc as locus A and B, respectively. From Eq. (4), it is approximately fulfilled that $\frac{\tau_{0A}}{\tau_{0B}} \cong \frac{D_{50A}}{D_{50B}}$. Similarly, the critical Shields stress of the median diameter in the two verticals is almost identical, i.e., $\frac{\tau_{*c50A}}{\tau_{*c50B}} \cong 1$ (as observed in Section 4.5.1). If additionally we consider that $b\cong1$ in Eq. (3), because the bed material in both verticals is close to equal mobility as shown in Section 4.5.1, then Eq. (3) together

with Eqs. (10) and (11) results in: $K_o \cong K_c \cong \frac{D_{50A}}{D_{50B}}$. In this case, Eq. (9) can be reduced to the form:

$$r_{iAB} = \frac{F_{iA}}{F_{iB}}\left(\frac{D_{50A}}{D_{50B}}\right)^{\frac{3}{2}} \qquad (12)$$

which states that the difference in mobility between A and B is exclusively determined by the median diameters as well as the relative abundance of the given grain size fraction in the bed material in each location.

Eq. (12) has been applied to the different grain size classes in the sediment sampled in the Ib and Ib-Cc verticals. For that purpose, the subsurface material F_i has been used because the superficial material contains a narrower spectrum of grain sizes due to limitations of the sampling method. Results are illustrated in Figure 10a, where values obtained from measured fractional transport rates at different water discharge classes are shown as well. The computed trend is consistent with the measured data. Particularly, for the lowest discharge class (773 m^3/s) a quite good agreement between measured and computed values is evident. These results reveal that grain sizes < 8 mm have a greater mobility in the Ib-Cc vertical than in Cc, while particles > 8 mm are more mobile in the Cc vertical than in the Ib-Cc. At flow stages higher than the 862 m^3/s discharge class, the measured data in Ib-Cc reveal a strong increment of the mobility of size fractions lower than 1 mm with respect to Cc, which is not captured by the computations. This trend is a response to the abrupt change in texture in Ib-Cc, already evidenced in Figure 7. Similarly, at the Cc vertical and for the two largest discharge classes, there is a strong disagreement between the computed and measured curves of Figure 10a, likely related to an increase of grain size fractions between 2 and 8 mm in the transported material in Cc.

Eq. (9) has been applied to compare the Ob and Cc verticals. Bed shear stress as a function of channel discharge has been obtained from the relations given in Table 3, and the critical shear stresses have been computed from Eq. (3) using b=0.87, i.e., assuming an almost equal mobility of all size fractions. τ_{*c50} for the Cc was the value obtained in Section 4.5.1, while for the Ob different values were used in order to show the effect of this parameter on the computations. Results for Q_w=900 m^3/s are shown in Figure 10b. The computed values from the comparison between Ib-Cc and Cc are plotted in the same

graphic as a reference. The results in Figure 10b give evidence of the key role that the critical Shields stress of the median diameter would have on the mobility of sediment at the Ob vertical. Very low τ_{*c50} values, close to the lower limit between 0.01 and 0.03 reported for poorly sorted sediment mixtures by different authors (e.g., Buffington & Montgomery, 1997; Ferreira et al., 2015; Petit et al., 2015) result in grain sizes roughly larger than 3 mm being more mobile in the Ob than in the Cc. Conversely, for values of τ_{*c50} larger than 0.04, all the grain size fractions result to be more mobile in the Cc than the Ob, so that for these conditions the total bed load would be larger at the Cc than at the Ob.

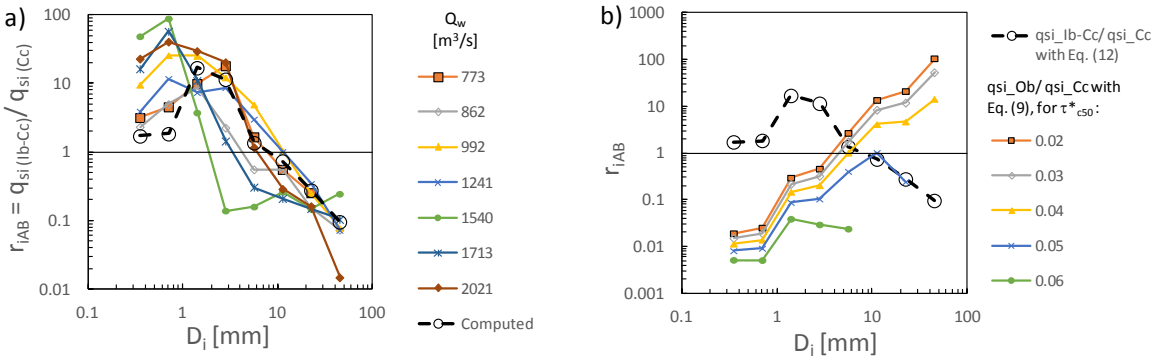

Figure 10 Relative mobility of grain size fractions, in the Ib-Cc vertical with respect to the Cc (a) for measured and computed values; and in the Ob vertical with respect to the Cc (b), as a function of the critical Shields stress for the median diameter.

In summary, at low flow stages over the point bar the mobility of a given grain size responds to its relative local abundance and the local median diameter, while at larger flow stages local differences in the mobility of grain sizes occur, probably related to changes in sediment supply. In the pool, if the critical Shields stress is of the same magnitude as in the point bar, size fractions coarser than roughly 4 mm are more mobile than over the point bar. Nevertheless, since the mobility of the bed material is strongly tied to the incipient motion, bed structuring and armoring development could induce for some conditions a lower mobility of coarse size fractions in the pool than over the point bar. In this latter case, the locus of maximum total bed load would not match with the locus of maximum shear stress.

6. DISCUSSION

Systematic bed load measurements at meander bends in gravel bed streams are scarce (e.g., Dietrich & Whiting, 1989; Julien & Anthony, 2002; Clayton & Pitlick, 2007), and as far as we know, none of these pertains to a large gravel bed river. Practical difficulties imposed by these environments in carrying out detailed measurements of hydraulic parameters and sediment sampling are some of the main reasons for bends in large gravel bed rivers being largely overlooked by researchers (Chapuis et al., 2015). Hence, the data set presented in this study represents a great opportunity to give some insight to identify those processes that promote morphodynamic stability at different temporal and spatial scales in this type of cross-section. We believe that such processes, as for instance crosswise grain-size sorting, would be more clearly defined in a large river, in comparison to small streams where local processes might overlap and be overshadowed by larger scatter. Therefore, even though we have only analyzed in detail two verticals in a cross-section, the large number of samples and the range of sampled flows (from 0.6 to 1.8 bankfull discharge) have contributed to reveal some well-defined patterns, which provide hints regarding the stability and the sediment transport mechanics in meander bends with heterogeneous bed material.

6.1 Morphological changes in the cross-section

A remarkable feature of the cross-section morphology during the study period was the vertical growth of the point bar while the adjacent pool remained mostly stable (Fig. 3). Some evidence indicates that the bar was largely eroded during the 2008 flood (the first and largest flood sampled). We suggest that the lateral confinement of the channel by vertical walls along the bend reach may contribute to an enhancement of the erosive action. In the study bend, floods larger than bankfull do not spill over the floodplain as is the case for unconfined sections upstream and downstream. Hence, the bed shear stress might continue increasing in pace with the channel discharge, and thus promote an excess in transport capacity not counterbalanced by sediment supply from upstream reaches. The large flood of 2008 must have thus readjusted the morphology of the bar and established non-equilibrium conditions for lower flow stages.

After the large event of 2008, the bar grew to almost recover, after 5 years, the bed level as before the large flood. We were able to relate the bar growth mainly to two

730 subsequent floods: the first not larger than bankfull (year 2009), and the second with some
731 peaks up to 30% larger than the bankfull discharge (year 2013). The significant role of
732 flows up to bankfull in point bar development has been highlighted by previous field
733 studies in meandering rivers (e.g., Legleiter et al., 2011; Kasvi et al., 2015). Also, in
734 observations of long term patterns of channel migration, Pizzuto (1994) reported on
735 intermediate discharges (1.2 to 2.7 year recurrence intervals) favoring deposition at the
736 inside of bends. Even for early stages of bar development, bar growth is enhanced by
737 topographic features that alter the direction of boundary shear stresses and sediment
738 transport (Legleiter et al., 2011). Dietrich & Smith (1984) suggested that the stability of a
739 point bar is strongly related to the convective accelerations that affect the direction of the
740 near bed flow velocity fields. Growth of the bar would occur due to a larger supply than the
741 flow capacity to remove sediment, up to a condition for which convective accelerations,
742 related to downstream shoaling over the bar, force the near bed flow direction toward the
743 outer bank. This reversing of flow would induce cross-stream sediment transport toward the
744 pool, and thus stabilize the point bar. An increase in stage, departing from the equilibrium
745 flow condition, would reduce the shoaling effect, allowing the development of an inward
746 flow component over the bar top (Dietrich & Whitting, 1989).

747 Growth of the point bar during flows lower than bankfull is indirectly confirmed by
748 fractional transport rates in the Ib-Cc vertical (shown in Fig. 7): for flows larger than
749 bankfull, bed load samples collected in this vertical showed a massive abundance of fine
750 material that was not evident either in the bed substrata or in bed load for lower flow stages.
751 In contrast, during low discharges, the subsurface material and bed load shared a similar
752 GSD. From this point of view, we suggest that the material rebuilding the point bar was
753 also related to flow stages lower than bankfull (when the shoaling effect described by
754 Dietrich & Smith [1984] was not relevant), and that fines in transport for discharges higher
755 than bankfull might thus have only been transferred through the Ib-Cc vertical on their way
756 to the bar front downstream or to the inner-bank.

757 The likely cyclic behavior on the point bar construction (for up to bankfull flows)
758 and degradation (during flow stages roughly exceeding 1.5 times the bankfull flow), gives
759 evidence of a tendency toward dynamic stability of the cross-section, but also, that the

channel bed is still very active in spite of the retention of sediment by the extensive damming of the river (Rovira et al., 2015), with the closest dam more than 70 km upstream of the study site. In the river reach downstream of dams, Vericat & Batalla (2006) found that the bed channel of the Ebro river was still active and relatively unstable, even after 40 years of damming with the resulting cutoff of bed load supply. They suggest that the period for a large system like the Ebro river, to adjust to dam regulation, would be in the order of a 100 year time-scale. It may be expected that in our study bend, as sediment supply decreases and a persistent armour layer is developed in the immediate reaches upstream, the point bar will be less able to recover after being eroded by very large floods.

6.2 Incipient motion and sediment transport

Our results indicate that threshold conditions for sediment motion are uniformly met over the point bar, since Cc and Ib-Cc verticals showed a strong equal mobility trend. A better correlation between local boundary shear stress and local bed material in Cc and Ib-Cc was found using the surface bed material, than using the subsurface particles. Thus, the equalized mobility may not include the fine size fractions present in the latter ($D<8$ mm). However, in the two verticals all particles would begin movement at a very narrow range of flow discharges in the channel, since incipient motion of fine material was observed occurs at flow discharges higher than 620 m^3/s, and the threshold of coarse size fractions occurs at flow discharges between 700 and 900 m^3/s according to the largest-grain method. Hence, a strong trend toward equal mobility is observed even when there is a two-fold difference between median grain sizes and local boundary shear at the two verticals. This symmetry allows the anticipation of the relative mobility of a given grain size, between the two verticals, by a simple relation considering the median diameters ratio and the relative abundance of the grain size fraction at each site (Eq. [12]) for low flow stages.

While the bar grew during the study period, the pool profile was approximately conserved, giving evidence of a balance between sediment transport capacity and supply. To achieve stability in gravel bed streams, spatially varied shear stress can be accommodated through grain size sorting and sediment flux adjustments (Powell, 1998). We suspect that the stability of the pool was related to a greater extend to the former, and also to other effects acting on the surface material characteristics to increase the threshold

for movement, such as armouring and bed surface structuring. The Ob vertical was the only one of the sampled verticals that exhibited a certain degree of armouring (although subtle, average ratio surface/subsurface for D_{16}, D_{50} and D_{84} is 1.31), and we cannot rule out that the bed could have gained in structuring through the passage of moderate floods with low excess of Shields stress (Church et al., 1998). As shown in Figure 10b, the bed load sediment transport rates in the Ob vertical are strongly linked to the critical Shields stress of the median sediment diameter τ_{*c50}. Due to armouring and structuring, we believe that τ_{*c50} in the Ob would have been much larger than in the recently deposited surface material in the Cc and Ib-Cc verticals. Hence, even when the highest boundary shear stresses from the four measuring verticals were measured at the Ob, if the pool region was characterized by high values of τ_{*c50} due to armouring and structuring, the zone of maximum bed load across the section would not match with the locus of maximum shear (for $\tau_{*c50} \geq 0.05$, all the grain sizes in the Ob would move at a lower rate than in the Cc, as shown in Fig. 10b). Some authors have found that the zone of maximum shear along bends does not necessarily match with the zone of maximum transport, either in sand or gravel bed streams (e.g., Dietrich & Whiting, 1989; Clayton & Pitlick, 2007). Hence, the stability of the pool might have been related to a low excess shear stress forced by high incipient motion thresholds required to mobilize the bed surface material. These high thresholds, and probably cross-stream transport directed to the pool, would have avoided bed erosion, and large boundary shear stresses in relation to the supplied material would have prevented sedimentation.

For bankfull and higher flow stages, selective transport of fine sediment occurred at the Ib-Cc and Ib verticals due to an excess of fines in the bed load in relation to the local bed material. It is most likely that this systematic inward fining trend of the bed load is related to the intensification of cross-stream sediment fluxes. Dietrich & Smith (1983) showed that the direction of the cross-stream flow velocity at the bed level can be strongly affected by flow stage and degree of development of a point bar. Under low flow stages there is a shoaling effect over the bar due to convective accelerations and pressure gradients, which directs the velocity vector outwards, to the pool. Nevertheless, for larger flow stages, when shoaling is no longer important, the vector direction may be reversed toward the bar. In a similar sense, it has been suggested that the role of cross-circulation in determining the shape of river bends is only important if the width-to-depth ratio is

sufficiently small (e.g., da Silva, 2015). In our study reach, a change in direction of velocity vectors when the shoaling effect lessens, or a strong intensification of the secondary circulation when the width-to-depth ratio decreases with flow stage, may thus activate the inward delivery of large quantities of fines over the bar, downstream of the bend apex where the pool is deepest (see Fig. 3).

An alternative explanation for the excess of fines in the bed load over the middle and inner bar sections would be the transfer to the inner bank of sediment traveling in suspension. Sand may be put in suspension at the upstream part of bends, where the maximum bed shear stress occurs near the channel center, and be guided onto the bar where it may travel as bed load due to the rapid decline of boundary shear (Dietrich & Whiting, 1989; Braudrick et al., 2009). Such a mechanism may have prompted bed load fining at Ib-Cc, even when the onset of bed load fining matches with flow conditions required for suspension of precisely the overrepresented size fractions (D=0.35 mm and 0.71 mm, see Fig. 4). Dietrich & Whiting (1989) considered that the strong crosswise variation in local boundary shear stress in river bends, may cause significant portions of the bed load to be composed of sand at high flow, for conditions in which this sediment would otherwise be carried in suspension. This mechanism could also explain the absence of fines in bed load samples at Cc, where larger bed shear stresses in comparison to Ib-Cc (a roughly two fold difference), would have kept the fine sediment in suspension.

The validity of the aforementioned mechanisms to explain the massive arrival of fines to the middle of the point bar (Ib-Cc) at flows larger than bankfull, and the persistence of the resulting bimodal GSD in the transported material at all flow stages above this threshold, cannot be proved with our data. This is a critical point that deserves to be clarified by further studies in view of the importance that fine material may have for the maintenance of non-constrained coarse bedded meanders; e.g., fine material directed to the inner-bank contributes to floodplain formation (Parker et al., 2011; Schuurman et al., 2015), and also, deposition of fines can plug the chutes that may disconnect the bar from the floodplain, where a new channel cutoff could otherwise be developed (Braudrick et al., 2009).

Finally, for the outliers in the sediment transport plots of Figures 5, 6 and 7, exhibiting high and coarse bed load rates for relatively low boundary shear stresses, a likely explanation, as already warned above, may be hysteresis effects in response to changing flow conditions. All these outliers occurred during the lower part of the falling limb of the hydrograph, when a rapid decline of stage could have caused a lag on the transport. Nevertheless, other causes for hysteresis, as changes in the surface grain size distribution or changes in sediment supply from the basin, as reported for bed load in some other studies (e.g., Kuhnle, 1992; Mao et al., 2014), cannot be discounted.

6.3 Sediment transport processes and adjustments promoting stability

Our results give evidence of processes acting at three different scales to achieve the stability of the river bend. At the local scale the median diameter of the surface material controls the mobility of the local sediment mixture, through hiding and exposure effects; additionally, in the pool, the development of an armour layer and structuring of the particles may delay the beginning of movement adding stability to the bed by reducing the local excess shear stress. At the cross-section scale, the bed topography controls the shear stress distribution, while bed material sorting accommodates mixtures with a coarse (fine) median diameter in zones of high (low) shear. The action of local and cross-section processes results in a quasi-equal mobility trend, at least over the point bar, of all grain size fractions with respect to the water stage in the channel. Our findings are complemented by the results of Clayton & Pitlick (2007), who suggested that, at the reach scale, the bend shape stability over long timescales is balanced by a roughly equivalent amount of sediment routed to different regions across the channel. At this scale it is relevant to consider the channel geometry, the flow velocity field and the net-cross stream sediment transport. The latter contributes to distribute sediment along the bend and adjust the morphology to changes in sediment supply and flow conditions.

Our initial hypothesis is partly valid. Processes that sustain bed stability in straight reaches are also active in meander bends. However, cross-stream sediment fluxes that are enhanced by secondary currents in curved beds and bed topography, may be of less importance in straight reaches. In the analysed cross-section, we have found that in controlling the relationship between boundary shear stress and bed load transport fields,

grain size adjustments dominate for conditions close to incipient motion, so that all size fractions begin to move within a narrow range of flow stages. Conversely, for flow stages larger than bankfull, cross-stream sediment transport may dominate over grain size adjustments.

Simulations of climate change scenarios indicate that the effect on sediment fluxes may be amplified in comparison to the driving rainfall and discharge changes (Coulthard et al., 2012). However, the geomorphic response is nonlinear and strongly dependent on the change in thresholds of sediment movement (Praskievicz, 2015). In a meander bend of non-uniform sediment there is the potential for manifold interactions and coupling between the topography, bed surface texture and structuring, flow and sediment fluxes. All this complexity adds great uncertainty to our predictions for the response after an imbalance is induced in the system. For instance, under a hypothetic climate change scenario with more frequent large floods, we could expect that the point bar in the study cross-section would be eroded, and would not be able to recover if the frequency of erosive floods is larger than the frequency of regenerative events. However, such a response may not be valid if in the long term the bed surface stabilizes by the development of a persistent armour layer.

6. CONCLUSIONS

Based on bed material and bed load sampling, and measurements of flow in a cross-section at the end of a large river meander, we conclude that:

1. The morphology of the point bar in the study cross-section may follow a cyclic behavior of erosion-deposition, which highlights the role of moderate floods in point bar construction.
2. The succession with flow stage of partial mobility, selective transport and equal mobility of sediment mixtures, common in straight reaches, is not necessarily followed in some regions of curved channels. In our study reach the successive stages over the mid-region of the point bar were partial mobility at very low discharges when only very fine size fractions moved; equal mobility at low

discharges not far from the previous stage ($\tau_o/\tau_{c50} < 1.6$); and selective transport of fine material at high flow discharges ($\tau_o/\tau_{c50} > 1.6$).

3. A quasi-equal mobility with respect to flow discharge is achieved over the bend point bar, in spite of large crosswise differences in median grain size and absolute value of the local shear stresses. This is achieved through a strong correlation between local bed shear stress and bed surface texture.
4. The pool morphology remained stable during the study period. This is the region where the largest shear stress across the channel occurs. We suggest that bed surface armouring and bed structuring increases the stability in comparison to the point bar. For large flow stages, it is likely that sediment transport convergence, mainly due to gravity flows from the bar, would also contribute to a stable pool morphology.
5. Processes that sustain bed stability in straight reaches are also active in meander bends, although in the latter, cross-stream sediment fluxes may largely contribute to increase the supply of sediment to the zones of high boundary shear stress. We identified the following processes acting at different scales to induce stability: at the local scale surface armouring and hiding-exposure induce an equal mobility of size fractions, so that the median diameter of the surface material controls the mobility of the local sediment mixture; at the cross-section scale, the bed topography controls the shear stress distribution, and sediment sorting ensures that local boundary shear stress correlates with local grain sizes; at the reach scale the channel geometry, flow velocity field and sediment differential routing intervene to sort sediment through regions of more efficient transportation.
6. In the analysed cross-section, in controlling the relationship between boundary shear stress and bed load transport fields, grain size adjustments dominate for conditions close to incipient motion, so that all size fractions begin to move within a narrow range of flow stages. Conversely, for flow stages larger than bankfull, cross-stream sediment transport dominates over grain size adjustments, so that fines are massively transferred inward.

Acknowledgements

This work was carried out within the research project CGL2008-01442 funded by the Spanish Ministry of Science and Innovation and the Water Catalan Authorities (ACA). Authors are indebted to Lluis Jornet and David Mateu for their assistance during field work. Substantial improvements to an earlier version of this manuscript were possible thanks to the thoughtful suggestions and comments from two anonymous reviewers, to whom the authors greatly acknowledge.

References

Andrews, E. D. (1983). Entrainment of gravel from naturally sorted riverbed material. *Geological Society of America Bulletin*, *94*(10), 1225-1231.

Andrews, E. D., & Parker, G. (1987). Formation of a coarse surface layer as the response to gravel mobility. *Sediment Transfer in Gravel-Bed Rivers. John Wiley & Sons New York. 1987. p 269-300*

Ashworth, P. J., & Ferguson, R. I. (1989). Size-selective entrainment of bed load in gravel bed streams. *Water Resources Research*, *25*(4), 627-634.

Batalla, R. J., Gomez, C. M., & Kondolf, G. M. (2004). Reservoir-induced hydrological changes in the Ebro River basin (NE Spain). *Journal of Hydrology*, *290*(1), 117-136.

Batalla, R. J., & Martín-Vide, J. P. (2001). Thresholds of particle entrainment in a poorly sorted sandy gravel-bed river. *Catena*, *44*(3), 223-243.

Billi, P., & Paris, E. (1992). Bed sediment characterization in river engineering problems *Erosion and Sediment Transport Monitoring in River Basins*, Proceedings of the Oslo Symposium, *IAHS Publ. no. 210*, 11-20.

Blanckaert, K., & Graf, W. H. (2001). Mean flow and turbulence in open-channel bend. *Journal of Hydraulic Engineering*, *127*(10), 835-847.

Braudrick, C. A., Dietrich, W. E., Leverich, G. T., & Sklar, L. S. (2009). Experimental evidence for the conditions necessary to sustain meandering in coarse-bedded rivers. *Proceedings of the National Academy of Sciences*, *106*(40), 16936-16941.

Bridge, J.S. (1992). A revised model for water flow, sediment transport, bed topography and grain size sorting in natural river bends. Water Resour. Res. 28 (4), 999–1013.

967 Buffington, J. M., & Montgomery, D. R. (1997). A systematic analysis of eight decades of incipient
968 motion studies, with special reference to gravel-bedded rivers. *Water Resources Research*, *33*(8),
969 1993-2029.

970 Bunte, K., & Abt, S. R. (2001), Sampling surface and subsurface particle-size distributions in
971 wadable gravel- and cobble-bed streams for analyses in sediment transport, hydraulics, and
972 streambed monitoring, Gen. Tech. Rep. RMRS-GTR-74, *U.S. Dep. of Agric., For. Serv., Rocky Mt.*
973 *Res. Stn.*, Fort Collins, Colo.

974 Bunte, K., & Abt, S. R. (2009). *Transport relationships between bedload traps and a 3-inch Helley-*
975 *Smith sampler in coarse grav el-bed streams and development of adjustment functions*Completion
976 Report No. 218 (p. 138). Colorado Water Institute.

977 Bunte, K., Abt, S. R, Potyondy, J. P. & Swingle, K. W. (2008). A Comparison of Coarse Bedload
978 Transport Measured with Bedload Traps and Helley-Smith Samplers. *Geodinamica Acta* 21 (1-2),
979 53-66.

980 Carling, P. A. (1983). Threshold of coarse sediment transport in broad and narrow natural streams.
981 *Earth Surface Processes and Landforms*, *8*(1), 1-18.

982 Chapuis, M., Dufour, S., Provansal, M., Couvert, B., & De Linares, M. (2015). Coupling channel
983 evolution monitoring and RFID tracking in a large, wandering, gravel-bed river: Insights into
984 sediment routing on geomorphic continuity through a riffle–pool sequence. *Geomorphology*, *231*,
985 258-269.

986 Clayton, J. A., & Pitlick, J. (2007). Spatial and temporal variations in bed load transport intensity in
987 a gravel bed river bend. *Water Resources Research*, *43*(2).

988 Church, M., & Hassan, M. A. (2002). Mobility of bed material in Harris Creek. *Water Resources*
989 *Research*, *38*(11).

990 Church, M., Hassan, M. A., & Wolcott, J. F. (1998). Stabilizing self-organized structures in
991 gravel-bed stream channels: Field and experimental observations. *Water Resources Research*,
992 *34*(11), 3169-3179.

993 Church, M. A., McLean, D. G., & Wolcott, J. F. (1987). River bed gravels: sampling and analysis.
994 *Sediment Transport in Gravel-Bed Rivers. John Wiley and Sons New York. 1987. p 43-88*

995 Constantine, J. A., Dunne, T., Ahmed, J., Legleiter, C., & Lazarus, E. D. (2014). Sediment supply
996 as a driver of river meandering and floodplain evolution in the Amazon Basin. *Nature Geoscience*,
997 *7*(12), 899-903.

998 Coulthard, T. J., Ramirez, J., Fowler, H. J., & Glenis, V. (2012). Using the UKCP09 probabilistic
999 scenarios to model the amplified impact of climate change on drainage basin sediment yield.
1000 *Hydrology and Earth System Sciences*, *16*(11), 4401.

1001 da Silva, A. M. F. (2015). Recent advances from research on meandering and directions for future
1002 work. In *Rivers–Physical, Fluvial and Environmental Processes* (pp. 373-401). Springer
1003 International Publishing.

1004 da Silva, A. M. F., El-Tahawy, T., & Tape W. D. (2006). Variation of flow pattern with sinuosity in
1005 sine-generated meandering streams. Journal of Hydraulic Engineering, 132(10), 1003-1014

1006 Dietrich, W. E. (1982). Settling velocity of natural particles. *Water Resources Research*, *18*(6),
1007 1615-1626.

1008 Dietrich, W. E. (1987). Mechanics of flow and sediment transport in river bends. *River channels:*
1009 *Environment and process*, *134*, 179-227.

1010 Dietrich, W. E., & Smith, J. D. (1983). Influence of the point bar on flow through curved channels.
1011 *Water Resources Research*, *19*(5), 1173-1192.

1012 Dietrich, W. E., & Smith, J. D. (1984). Bed load transport in a river meander. *Water Resources*
1013 *Research*, *20*(10), 1355-1380.

1014 Dietrich, W. E., & Whiting, P. (1989). Boundary shear stress and sediment transport in river
1015 meanders of sand and gravel. *River meandering*, 1-50.

1016 Emmett, W.W. (1979). A field calibration of the sediment-trapping characteristics of the Helley-
1017 Smith bedload sampler. Open-File Report 79-411.

1018 Engelund, F. (1974). Flow and bed topography in channel bends. J Hydr Div 100(11):1631–1648

1019 Ferreira, R. M., Hassan, M. A., & Ferrer-Boix, C. (2015). Principles of bedload transport of non-
1020 cohesive sediment in open-channels. In *Rivers–Physical, Fluvial and Environmental Processes* (pp.
1021 323-372). Springer International Publishing.

1022 Ferrer-Boix, C., & Hassan, M. A. (2014). Influence of the sediment supply texture on
1023 morphological adjustments in gravel-bed rivers. *Water Resources Research*, *50*(11), 8868-8890.

Goode, J. R., Luce, C. H., & Buffington, J. M. (2012). Enhanced sediment delivery in a changing climate in semi-arid mountain basins: Implications for water resource management and aquatic habitat in the northern Rocky Mountains. *Geomorphology*, *139*, 1-15.

Hubbell, D. W. (1987). Bed load sampling and analysis. *Sediment Transport in Gravel-Bed Rivers. John Wiley and Sons New York. 1987. p 89-118*

Julien, P. Y., & Anthony, D. J. (2002). Bed load motion and grain sorting in a meandering stream. *Journal of Hydraulic Research*, *40*(2), 125-133.

Kasvi, E., Petteri, A., Matti, V., Hannu, H., & Juha, H. (2013). Spatial and temporal distribution of fluvio-morphological processes on a meander point bar during a flood event. *Hydrology Research*, *44*(6), 1022-1039.

Kasvi, E., Vaaja, M., Kaartinen, H., Kukko, A., Jaakkola, A., Flener, C., Hyyppä, H., Hyyppä, J., & Alho, P. (2015). Sub-bend scale flow–sediment interaction of meander bends—A combined approach of field observations, close-range remote sensing and computational modelling. *Geomorphology*, *238*, 119-134.

Komar, P. D. (1987). Selective gravel entrainment and the empirical evaluation of flow competence. *Sedimentology*, *34*(6), 1165-1176.

Kuhnle, R. A. (1992). Bed load transport during rising and falling stages on two small streams. *Earth Surface Processes and Landforms*, *17*(2), 191-197.

Kundzewicz ZW, Mata LJ, Arnell N, Döll P, Kabat P, Jiménez B, Miller K, Oki T, Şen Z, & Shiklomanov I. (2007). Freshwater resources and their management. In Climate Change 2007: Impacts, Adaptation and Vulnerability. Contribution of Working Group II to the Fourth Assessment Report of the Intergovernmental Panel on Climate Change, Parry ML, Canziani OF, Palutikof JP, van der Linden PJ, Hanson CE (eds). Cambridge University Press: Cambridge; 174–210.

Lanzoni, S., Siviglia, A., Frascati, A., & Seminara, G. (2006). Long waves in erodible channels and morphodynamic influence. *Water Resources Research*, 2006;42:W06D17.

Legleiter, C. J., Harrison, L. R., & Dunne, T. (2011). Effect of point bar development on the local force balance governing flow in a simple, meandering gravel bed river. *Journal of Geophysical Research: Earth Surface*, *116*(F1).

Lima, M. M. C. L. (2014). Shallow water flow around an elongated bridge pier. In *V Conferência Nacional de Mecânica dos Fluidos, Termodinâmica e Energia MEFTE 2014*, Porto, Portugal

1054 Lisle, T. E., Nelson, J. M., Pitlick, J., Madej, M. A., & Barkett, B. L. (2000). Variability of bed
1055 mobility in natural, gravel-bed channels and adjustments to sediment load at local and reach scales.
1056 *Water Resources Research*, *36*(12), 3743-3755.

1057 Lotsari, E., M. Vaaja, C. Flener, H. Kaartinen, A. Kukko, E. Kasvi, H. Hyyppä, J. Hyyppä, & P.
1058 Alho (2014). Annual bank and point bar morphodynamics of a meandering river determined by
1059 high-accuracy multitemporal laser scanning and flow data. *Water Resources Research*, *50*(7), 5532-
1060 5559.

1061 Mao, L., Dell'Agnese, A., Huincache, C., Penna, D., Engel, M., Niedrist, G., & Comiti, F. (2014).
1062 Bedload hysteresis in a glacier-fed mountain river. *Earth Surface Processes and Landforms*, *39*(7),
1063 964-976.

1064 Martín-Vide, J. P., Plana-Casado, A., Sambola, A., & Capapé, S. (2015). Bedload transport in a
1065 river confluence. *Geomorphology*, *250*, 15-28.

1066 Nelson, P. A., Venditti, J. G., Dietrich, W. E., Kirchner, J. W., Ikeda, H., Iseya, F., & Sklar, L. S.
1067 (2009). Response of bed surface patchiness to reductions in sediment supply. *Journal of*
1068 *Geophysical Research: Earth Surface*, *114*(F2).

1069 Nelson, P. A., Dietrich, W. E., & Venditti, J. G. (2010). Bed topography and the development of
1070 forced bed surface patches. *Journal of Geophysical Research: Earth Surface*, *115*(F4).

1071 Parker, G. (2007). Transport of gravel and sediment mixtures. In Sedimentation Engineering:
1072 Processes, Measurements, Modeling And Practice, Manual 110, Sedimentation Committee of the
1073 Environmental and Water Resources Institute, Garcia MH (ed.). American Society of Civil
1074 Engineers: Reston, VA; 165–251.

1075 Parker, G. & Andrews, E.D. (1985): Sorting of bedload sediments by flow in meander bends. Water
1076 Resources Research 21, 1361-73.

1077 Parker, G., & Klingeman, P. C. (1982), On why gravel bed streams are paved. *Water Resources*
1078 *Res*, *18*, 1409-14.

1079 Parker, G., Klingeman, P. C., & McLean, D. G. (1982). Bedload and size distribution in paved
1080 gravel-bed streams. *Journal of the Hydraulics Division*, *108*(4), 544-571.

1081 Parker, G., Shimizu, Y., Wilkerson, G. V., Eke, E. C., Abad, J. D., Lauer, J. W., Paola, C., Dietrich,
1082 W. E., & Voller, V. R. (2011). A new framework for modeling the migration of meandering rivers.
1083 *Earth Surface Processes and Landforms*, *36*(1), 70-86.

Petit, F., Houbrechts, G., Peeters, A., Hallot, E., Van Campenhout, J., & Denis, A. C. (2015). Dimensionless critical shear stress in gravel-bed rivers. *Geomorphology*, *250*, 308-320.

Pizzuto, J. E. (1994). Channel adjustments to changing discharges, Powder River, Montana. *Geological Society of America Bulletin*, *106*(11), 1494-1501.

Powell, D. M. (1998). Patterns and processes of sediment sorting in gravel-bed rivers. *Progress in Physical Geography*, *22*(1), 1-32.

Powell, D. M., Reid, I., & Laronne, J. B. (1999). Hydraulic interpretation of cross-stream variations in bed-load transport. *Journal of Hydraulic Engineering*, *125*(12), 1243-1252.

Praskievicz, S. (2015). A coupled hierarchical modeling approach to simulating the geomorphic response of river systems to anthropogenic climate change. *Earth Surface Processes and Landforms*, *40*(12), 1616-1630.

Reid, I., & Frostick, L. E. (1986). Dynamics of bedload transport in Turkey Brook, a coarse-grained alluvial channel. *Earth Surface Processes and Landforms*, *11*(2), 143-155.

Rovira, A., Ibáñez, C., & Martín-Vide, J.P. (2015). Suspended sediment load at the lowermost Ebro River (Catalonia, Spain). *Quaternary International*, 388, 188-198.

Schuurman, F., Shimizu, Y., Iwasaki, T., & Kleinhans, M. G. (2016). Dynamic meandering in response to upstream perturbations and floodplain formation. *Geomorphology*, *253*, 94-109.

Smith, J. D., & McLean, S. R. (1984) A model for flow in meandering streams. Water Resour Res 20(9):1301–1315

Sterling, S. M., & Church, M. (2002). Sediment trapping characteristics of a pit trap and the Helley-Smith sampler in a cobble gravel bed river. *Water Resources Research*, *38*(8).

Tabara, J. D., Roca, E., Madrid, C., Valkering, P., Wallman, P., & Weaver, P. (2008). Integrated sustainability assessment of water systems: lessons from the Ebro River Basin. *International journal of innovation and sustainable development*, *3*(1-2), 48-69.

Termini, D., & Piraino, M. (2011). Experimental analysis of cross-sectional flow motion in a large amplitude meandering bend. Earth Surf Process Landforms, 36(2):244–56.

Termini, D. (2015). Momentum transport and bed shear stress distribution in a meandering bend: Experimental analysis in a laboratory flume. *Advances in Water Resources*, *81*, 128-141.

1112 Van Dijk, W. M., Lageweg, W. I., & Kleinhans, M. G. (2012). Experimental meandering river with
1113 chute cutoffs. *Journal of Geophysical Research: Earth Surface*, *117*(F3).

1114 Vericat, D., & Batalla, R. J. (2005). Sediment transport in a highly regulated fluvial system during
1115 two consecutive floods (lower Ebro River, NE Iberian Peninsula). *Earth Surface Processes and*
1116 *Landforms*, *30*(4), 385-402.

1117 Vericat, D., Batalla, R. J., & Garcia, C. (2006). Breakup and reestablishment of the armour layer in
1118 a large gravel-bed river below dams: The lower Ebro. *Geomorphology*, *76*(1), 122-136.

1119 Vericat, D., Church, M., & Batalla, R. J. (2006). Bed load bias: Comparison of measurements
1120 obtained using two (76 and 152 mm) Helley-Smith samplers in a gravel bed river. *Water Resources*
1121 *Research*, 42, 1-13.

1122 Whitaker, A. C., & Potts, D. F. (2007). Analysis of flow competence in an alluvial gravel bed
1123 stream, Dupuyer Creek, Montana. *Water resources research*, *43*(7).

1124 Wilcock, P. R. (1988). Methods for estimating the critical shear stress of individual fractions in
1125 mixed-size sediment. *Water Resources Research*, *24*(7), 1127-1135.

1126 Wilcock, P. R. (1992). Flow competence: A criticism of a classic concept. *Earth Surface Processes*
1127 *and Landforms*, *17*(3), 289-298.

1128 Wilcock, P. R., & McArdell, B. W. (1993). Surface-based fractional transport rates: Mobilization
1129 thresholds and partial transport of a sand-gravel sediment. *Water Resources Research*, *29*(4), 1297-
1130 1312.

1131 Wilcock, P. R., & Southard, J. B. (1988). Experimental study of incipient motion in mixed-size
1132 sediment. *Water Resources Research*, *24*(7), 1137-1151.

1133 Yalin, M. S. (1992) River mechanics. Pergamon Press, London, UK